



# Computing nearly singular solutions using pseudo-spectral methods

Thomas Y. Hou<sup>a,b,\*</sup>, Ruo Li<sup>c</sup>

<sup>a</sup> *Applied and Computational Mathematics, 217-50, Caltech, Pasadena, CA 91125, USA*

<sup>b</sup> *LSEC, Academy of Mathematics and Systems Sciences, Chinese Academy of Sciences, Beijing 100080, China*

<sup>c</sup> *LMAM & School of Mathematical Sciences, Peking University, Beijing 100871, China*

Received 10 January 2007; accepted 13 April 2007

Available online 29 April 2007

---

## Abstract

In this paper, we investigate the performance of pseudo-spectral methods in computing nearly singular solutions of fluid dynamics equations. We consider two different ways of removing the aliasing errors in a pseudo-spectral method. The first one is the traditional  $2/3$  dealiasing rule. The second one is a high (36th) order Fourier smoothing which keeps a significant portion of the Fourier modes beyond the  $2/3$  cut-off point in the Fourier spectrum for the  $2/3$  dealiasing method. Both the 1D Burgers equation and the 3D incompressible Euler equations are considered. We demonstrate that the pseudo-spectral method with the high order Fourier smoothing gives a much better performance than the pseudo-spectral method with the  $2/3$  dealiasing rule. Moreover, we show that the high order Fourier smoothing method captures about 12–15% more effective Fourier modes in each dimension than the  $2/3$  dealiasing method. For the 3D Euler equations, the gain in the effective Fourier codes for the high order Fourier smoothing method can be as large as 20% over the  $2/3$  dealiasing method. Another interesting observation is that the error produced by the high order Fourier smoothing method is highly localized near the region where the solution is most singular, while the  $2/3$  dealiasing method tends to produce oscillations in the entire domain. The high order Fourier smoothing method is also found to be very stable dynamically. No high frequency instability has been observed. In the case of the 3D Euler equations, the energy is conserved up to at least six digits of accuracy throughout the computations.

© 2007 Elsevier Inc. All rights reserved.

*Keywords:* Pseudo spectral methods; Singular solutions; Incompressible flow; Dealiasing

---

## 1. Introduction

Pseudo-spectral methods have been one of the most commonly used numerical methods in solving nonlinear partial differential equations with periodic boundary conditions. Pseudo-spectral methods have the advantage of computing a nonlinear convection term very efficiently using the fast Fourier transform. On the other

---

\* Corresponding author. Address: Applied and Computational Mathematics, 217-50, Caltech, Pasadena, CA 91125, USA.

E-mail addresses: [hou@acm.caltech.edu](mailto:hou@acm.caltech.edu) (T.Y. Hou), [rli@acm.caltech.edu](mailto:rli@acm.caltech.edu) (R. Li).

hand, the discrete Fourier transform of a periodic function introduces the so-called aliasing error [14,5,6,3], which is partially due to the artificial periodicity of the discrete Fourier coefficient as a function of the wave number. The aliasing error pollutes the accuracy of the high frequency modes, especially those last 1/3 of the high frequency modes. Without using any dealiasing or Fourier smoothing, the pseudo-spectral method may suffer from some mild numerical instability [13]. One of the most commonly used dealiasing methods is the so-called 2/3 dealiasing rule, in which one sets to zero the last 1/3 of the high frequency modes and keeps the first 2/3 of the Fourier modes unchanged. Another way to control the aliasing errors is to apply a smooth cut-off function or Fourier smoothing to the Fourier coefficients. However, many existing Fourier smoothing methods damp the last 1/3 of the high frequency modes just like the 2/3 dealiasing method.

In this paper, we investigate the performance of pseudo-spectral methods using the 2/3 dealiasing rule and a high order Fourier smoothing. In the Fourier smoothing method, we use a 36th order Fourier smoothing function which keeps a significant portion of the Fourier modes beyond the 2/3 cut-off point in the Fourier spectrum for the 2/3 dealiasing rule. We apply these two methods to compute nearly singular solutions in fluid flows. Both the 1D Burgers equation and the 3D incompressible Euler equations will be considered. The advantage of using the Burgers equation is that it shares some essential difficulties as other fluid dynamics equations, and yet we have a semi-analytic formulation for its solution. By using the Newton iterative method, we can obtain an approximate solution to the exact solution up to 13 digits of accuracy. Moreover, we know exactly when a shock singularity will form in time. This enables us to perform a careful convergence study in both the physical space and the spectral space very close to the singularity time.

We first perform a careful convergence study of the two pseudo-spectral methods in both physical and spectral spaces for the 1D Burgers equation. Our extensive numerical results demonstrate that the pseudo-spectral method with the high order Fourier smoothing (the Fourier smoothing method for short) gives a much better performance than the pseudo-spectral method with the 2/3 dealiasing rule (the 2/3 dealiasing method for short). In particular, we show that the unfiltered high frequency coefficients in the Fourier smoothing method approximate accurately the corresponding exact Fourier coefficients. More precisely, we demonstrate that the Fourier smoothing method captures about 12–15% more effective Fourier modes than the 2/3 dealiasing method in each dimension. The gain is even higher for the 3D Euler equations since the number of effective modes in the Fourier smoothing method is higher in three dimensions. Thus the Fourier smoothing method gives a more accurate approximation than the 2/3 dealiasing method. We will illustrate this improved accuracy by studying the errors in  $L^\infty$ -norm and  $L^1$ -norm as a function of time, and by studying the spatial distribution of the pointwise error and the convergence of the Fourier spectrum at a sequence of times very close to the singularity time. Another interesting observation is that the error produced by the Fourier smoothing method is highly localized near the region where the solution is most singular and decays exponentially fast with respect to the distance from the singularity point. The error in the smooth region is several orders of magnitude smaller than that in the singular region. On the other hand, the 2/3 dealiasing method produces noticeable oscillations in the entire domain as we approach the singularity time. This is to some extent due to the Gibbs phenomenon and the loss of the  $L^2$  energy associated with the solution. Moreover, our computational results show that in the smooth region the error produced by the Fourier smoothing method is several orders of magnitude smaller than that produced by the 2/3 dealiasing method. This is an important advantage of the Fourier smoothing method over the 2/3 dealiasing method.

Next, we apply the two pseudo-spectral methods to solve the nearly singular solution of the 3D incompressible Euler equations. We would like to see if the comparison we make regarding the convergence properties of the two pseudo-spectral methods for the 1D Burgers equation is still valid for the more challenging 3D incompressible Euler equations. In order to make our comparison meaningful, we choose a smooth initial condition which could potentially develop a finite time singularity. There have been many computational efforts in searching for finite time singularities of the 3D Euler equations, see e.g. [7,27,20,16,28,18,4,2,12,26,15,19]. One of the frequently cited numerical evidences for a finite time blowup of the Euler equations is the two slightly perturbed anti-parallel vortex tubes initial data studied by Kerr [18,19]. In Kerr's computations, a pseudo-spectral discretization with the 2/3 dealiasing rule was used in the  $x$  and  $y$  directions while a Chebyshev polynomial discretization was used along the  $z$  direction. His best space resolution was of the order  $512 \times 256 \times 192$ . In [18,19], Kerr reported that the maximum vorticity blows up like  $O((T-t)^{-1})$  and the velocity field blows up like  $O((T-t)^{-1/2})$ . The alleged singularity time  $T$  is equal to 18.7 while his

computations beyond  $t = 17$  were not considered as the primary evidence for a singularity since they were polluted by noises [18].

We perform a careful convergence study of the two pseudo-spectral methods using Kerr's initial condition with a sequence of resolutions up to  $T = 19$ , beyond the singularity time alleged in [18,19]. The largest space resolution we use is  $1536 \times 1024 \times 3072$ . Convergence in both physical and spectral space has been observed for the two pseudo-spectral methods. Both numerical methods converge to the same solution under mesh refinement. Our computational study also demonstrates that the Fourier smoothing method offers better computational accuracy than the 2/3 dealiasing method. For a given resolution, the Fourier smoothing method captures about 20% more effective Fourier modes than the 2/3 dealiasing method does. We also find that the 2/3 dealiasing method produces some oscillations near the 2/3 cut-off point of the spectrum. This abrupt cut-off of the Fourier spectrum generates noticeable oscillations in the vorticity contours at later times. Even using a relative high resolution  $1024 \times 786 \times 2048$ , we find that the vorticity contours obtained by the 2/3 dealiasing method still suffer relatively large oscillations in the late stage of the computations, which are to some extent caused by the Gibbs phenomenon and the loss of enstrophy due to the abrupt cut-off of the high frequency modes. On the other hand, the vorticity contours obtained by the Fourier smoothing method remains smooth throughout the computations. Our spectral computations using both the 2/3 dealiasing rule and the high order Fourier smoothing confirm the finding reported in [17], i.e. the maximum vorticity does not grow faster than double exponential in time and the velocity field remains bounded up to  $T = 19$ .

We would like to emphasize that the Fourier smoothing method is very stable and robust in all our computational experiments. We do not observe any high frequency instability in our computations for both the 1D Burgers equation and the 3D incompressible Euler equations. In the case of the 3D Euler equations, the energy is conserved up to at least six digits of accuracy throughout the computations. The resolution study that we conduct is completely based on the consideration of accuracy, not by the consideration of stability.

We would like to mention that Fourier smoothing has been also used effectively to approximate discontinuous solutions of linear hyperbolic equations, see e.g. [23,25,1]. To compute discontinuous solutions for non-linear conservation laws, the spectral viscosity method has been introduced and analyzed, see [29,22] and the review article [30]. Like Fourier smoothing, the purpose of introducing the spectral viscosity is to localize the Gibbs oscillations, maintaining stability without loss of spectral accuracy.

The remaining of the paper is organized as follows. In Section 2, we present a careful convergence study of the two pseudo-spectral methods for the 1D Burgers equation. In Section 3, we present a similar convergence study for the incompressible 3D Euler equations using Kerr's initial data. Some concluding remarks are made in Section 4.

## 2. Convergence study of the two pseudo-spectral methods for the 1D Burgers equation

In this section, we perform a careful convergence study of the two pseudo-spectral methods for the 1D Burgers equation. The 1D Burgers equation shares some of the essential difficulties in many fluid dynamic equations. In particular, it has the same type of quadratic nonlinear convection term as other fluid dynamics equations. It is well known that the 1D Burgers equation can form a shock discontinuity in a finite time [21]. The advantage of using the 1D Burgers equation as a prototype is that we have a semi-analytical solution formulation for the 1D Burgers equation. This allows us to use the Newton iterative method to obtain a very accurate approximation (up to 13 digits of accuracy) to the exact solution of the 1D Burgers equation arbitrarily close to the singularity time. This provides a solid foundation in our convergence study of the two spectral methods.

We consider the inviscid 1D Burgers equation

$$u_t + \left(\frac{u^2}{2}\right)_x = 0, \quad -\pi \leq x \leq \pi, \quad (1)$$

with an initial condition given by

$$u|_{t=0} = u_0(x).$$

We impose a periodic boundary condition over  $[-\pi, \pi]$ . By the method of characteristics, it is easy to show that the solution of the 1D Burgers equation is given by

$$u(x, t) = u_0(x - tu(x, t)). \tag{2}$$

The above implicit formulation defines a unique solution for  $u(x, t)$  up to the time when the first shock singularity develops. After the shock singularity develops, Eq. (2) gives a multi-valued solution. An entropy condition is required to select a unique physical solution beyond the shock singularity [21].

We now use a standard pseudo-spectral method to approximate the solution. Let  $N$  be an integer, and let  $h = \pi/N$ . We denote by  $x_j = jh$  ( $j = -N, \dots, N$ ) the discrete mesh over the interval  $[-\pi, \pi]$ . To describe the pseudo-spectral methods, we recall that the discrete Fourier transform of a periodic function  $u(x)$  with period  $2\pi$  is defined by

$$\hat{u}_k = \frac{1}{2N} \sum_{j=-N+1}^N u(x_j) e^{-ikx_j}.$$

The inversion formula reads

$$u(x_j) = \sum_{k=-N+1}^N \hat{u}_k e^{ikx_j}.$$

We note that  $\hat{u}_k$  is periodic in  $k$  with period  $2N$ . This is an artifact of the discrete Fourier transform, and the source of the aliasing error. To remove the aliasing error, one usually applies some kind of dealiasing filtering when we compute the discrete derivative. Let  $\rho(k/N)$  be a cut-off function in the spectrum space. A discrete derivative operator may be expressed in the Fourier transform as

$$(\widehat{D_h u})_k = ik\rho(k/N)\hat{u}_k, \quad k = -N + 1, \dots, N. \tag{3}$$

Both the 2/3 dealiasing rule and the Fourier smoothing method can be described by a specific choice of the high frequency cut-off function,  $\rho$  (also known as Fourier filter). For the 2/3 dealiasing rule, the cut-off function is chosen to be

$$\rho(k/N) = \begin{cases} 1 & \text{if } |k/N| \leq 2/3, \\ 0 & \text{if } |k/N| > 2/3. \end{cases} \tag{4}$$

In our computations, in order to obtain an alias-free computation on a grid of  $M$  points for a quadratic nonlinear equation, we apply the above filter to the high wavenumbers so as to retain only  $(2/3)M$  unfiltered wavenumbers before making the coefficient-to-grid fast Fourier transform. This dealiasing procedure is alternatively known as the 3/2 dealiasing rule because to obtain  $M$  unfiltered wavenumbers, one must compute nonlinear products in physical space on a grid of  $(3/2)M$  points, see page 229 of [3] for more discussions.

For the Fourier smoothing method, we choose  $\rho$  as follows:

$$\rho(k/N) = e^{-\alpha(|k|/N)^m}, \tag{5}$$

with  $\alpha = 36$  and  $m = 36$ . In our implementation, both filters are applied on the numerical solution at every time step. For the 2/3 dealiasing rule, the Fourier modes with wavenumbers  $|k| \geq 2/3N$  are always set to zero. Thus there is no aliasing error being introduced in our approximation of the nonlinear convection term.

The Fourier smoothing method we choose is based on three considerations. The first one is that the aliasing instability is introduced by the highest frequency Fourier modes. As demonstrated in [13], as long as one can damp out a small portion of the highest frequency Fourier modes, the mild instability caused by the aliasing error can be under control. The second observation is that the magnitude of the Fourier coefficient is decreasing with respect to the wave number  $|k|$  for a function that has certain degree of regularity. Typically, we have  $|\hat{u}_k| \leq C/(1 + |k|)^m$  if the  $m$ th derivative of a function  $u$  is bounded in  $L^1$ . Thus the high frequency Fourier modes have a relatively smaller contribution to the overall solution than the low to intermediate frequency modes. The third observation is that one should not cut off high frequency Fourier modes abruptly to avoid the Gibbs phenomenon and the loss of the  $L^2$  energy associated with the solution. This is especially important when we compute a nearly singular solution whose high frequency Fourier coefficient has a very slow decay.

Based on the above considerations, we choose a smooth cut-off function which decays exponentially fast with respect to the high wave number. In our cut-off function, we choose the parameters  $\alpha = 36$  and  $m = 36$ . These two parameters are chosen to achieve two objectives: (i) When  $|k|$  is close to  $N$ , the cut-off function reaches the machine precision, i.e.  $10^{-16}$ . (ii) The cut-off function remains very close to 1 for  $|k| < 4N/5$ , and decays rapidly and smoothly to zero beyond  $|k| = 4N/5$ . In Fig. 1, we plot the cut-off function  $\rho(x)$  as a function of  $x$ . The cut-off function used by the 2/3rd dealiasing rule is plotted on top of the cut-off function used by the Fourier smoothing method. We can see that the Fourier smoothing method keeps about 12–15% more modes than the 2/3 dealiasing method. In this paper, we will demonstrate by our numerical experiments that the extra modes we keep by the Fourier smoothing method give an accurate approximation of the correct high frequency Fourier modes.

Next, we will present a convergence study of the two pseudo-spectral methods using a generic initial condition,  $u_0(x) = \sin(x)$ . For this initial condition, the solution will develop a shock singularity at  $t = 1$  at  $x = \pi$  and  $x = -\pi$ . For  $t < 1$  but sufficiently close to the singularity time, a sharp layer will develop at  $x = \pi$  and  $x = -\pi$ . We will perform a sequence of well-resolved computations sufficiently close to the singularity time using the two pseudo-spectral methods and study their convergence properties. In our computations for both methods, we will use a standard compact three step Runge–Kutta scheme for the time integration. In order to compute the errors of the two pseudo-spectral methods accurately, we need to solve for the “exact solution” on a computational grid. We do this by solving the implicit solution formula (2) using the Newton iterative method up to 13 digits of accuracy.

Our computational studies demonstrate convincingly that the Fourier smoothing method gives a much better performance than the 2/3 dealiasing method. In Fig. 2, we plot the  $L^\infty$  error of the two pseudo-spectral methods as a function of time using three different resolutions. The errors are plotted in a log–log scale. The left figure is the result obtained by the 2/3 dealiasing method and the right figure is the result obtained by the Fourier smoothing method. We can see clearly that the  $L^\infty$  error obtained by the Fourier smoothing method is smaller than that obtained by the 2/3rd dealiasing method. With increasing resolution, the errors obtained by both methods decay rapidly, confirming the spectral convergence of both methods. In Fig. 3, we plot the  $L^1$  errors of the two methods as a function of time using three different resolutions. We can see that the convergence of the Fourier smoothing method is much faster than the 2/3 dealiasing method.

It is interesting to study the spatial distribution of the pointwise errors obtained by the two methods. In Fig. 4, we plot the pointwise errors of the two methods over one period  $[-\pi, \pi]$  at  $t = 0.985$ . In the computations presented on the left picture, we use resolution  $N = 1024$ , while the computations in the right picture corresponds to  $N = 2048$ . The errors are plotted in a log scale. We can see that the error of the 2/3rd dealiasing method, which is colored in red, is highly oscillatory and spreads out over the entire domain. This is caused by

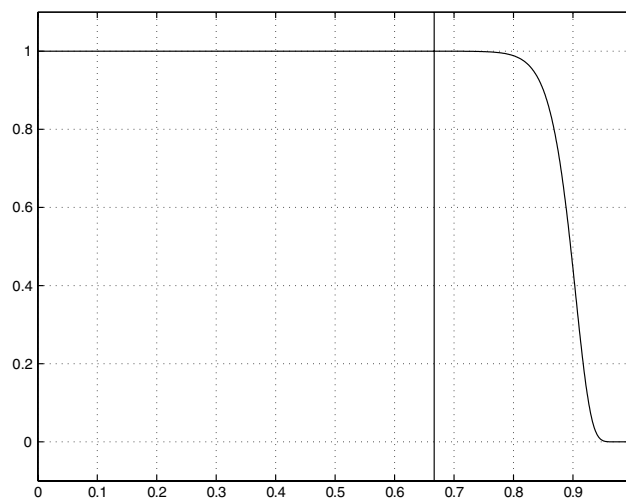


Fig. 1. The profile of the Fourier smoothing,  $\exp(-36(x)^{36})$ , as a function of  $x$ . The vertical line corresponds to the cut-off point in the Fourier spectrum in the 2/3 dealiasing rule. We can see that using this Fourier smoothing we keep about 12–15% more modes than those using the 2/3 dealiasing rule.

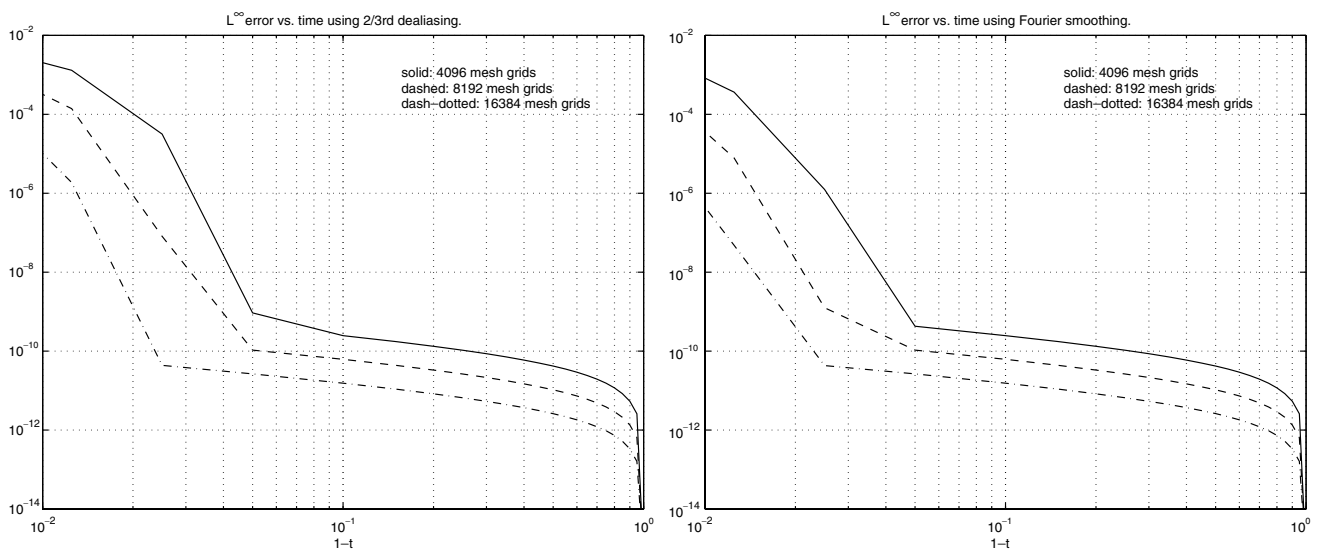


Fig. 2. The  $L^\infty$  errors of the two pseudo-spectral methods as a function of time using three different resolutions. The plot is in a log–log scale. The initial condition is  $u_0(x) = \sin(x)$ . The left figure is the result obtained by the 2/3 dealiasing method and the right figure is the result obtained by the Fourier smoothing method. It can be seen clearly that the  $L^\infty$  error obtained by the Fourier smoothing method is smaller than that obtained by the 2/3 dealiasing method.

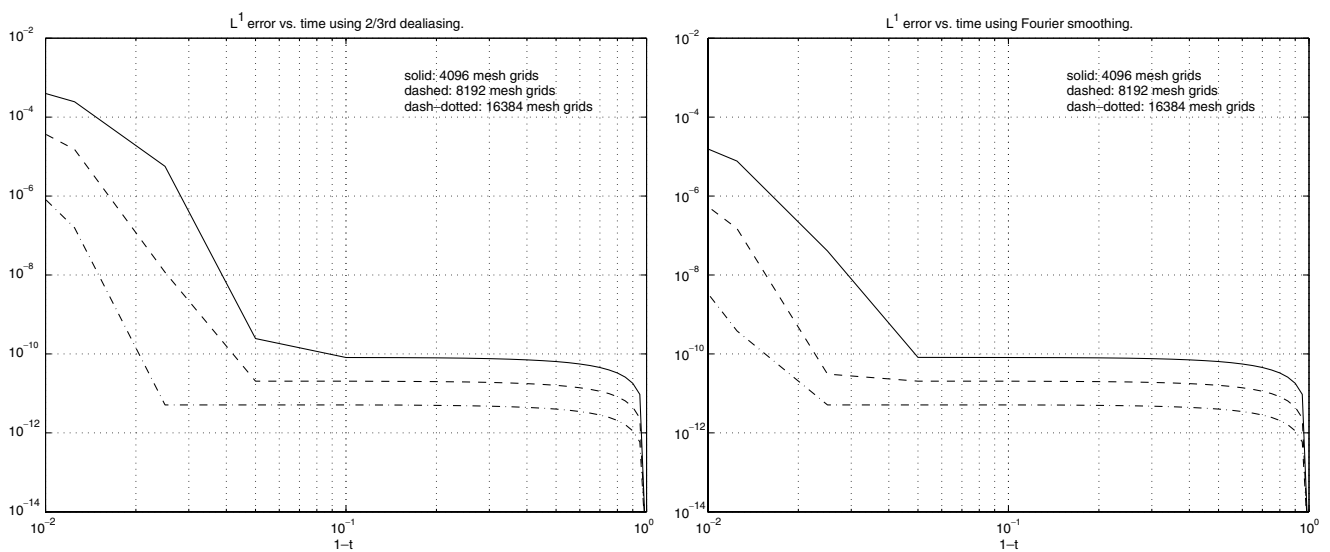


Fig. 3. The  $L^1$  errors of the two pseudo-spectral methods as a function of time using three different resolutions. The plot is in a log–log scale. The initial condition is given by  $u_0(x) = \sin(x)$ . The left figure is the result obtained by the 2/3 dealiasing method and the right figure is the result obtained by the Fourier smoothing method. One can see that the  $L^1$  error obtained by the Fourier smoothing method is much smaller than corresponding  $L^\infty$  error.

the Gibbs phenomenon and the loss of the  $L^2$  energy associated with the solution. On the other hand, the error of the Fourier smoothing method is highly localized near the location of the shock singularity at  $x = \pi$  and  $x = -\pi$ , and decays exponentially fast with respect to the distance from the singularity point. The error in the smooth region is several orders of magnitude smaller than that in the singular region. This is a very interesting phenomenon. This property makes the Fourier smoothing method a better method for computing nearly singular solutions.

To gain further insight of the two pseudo-spectral methods, we study the convergence of the two methods in the spectral space. In Fig. 5, we plot the Fourier spectra of the two spectral methods at a sequence of times

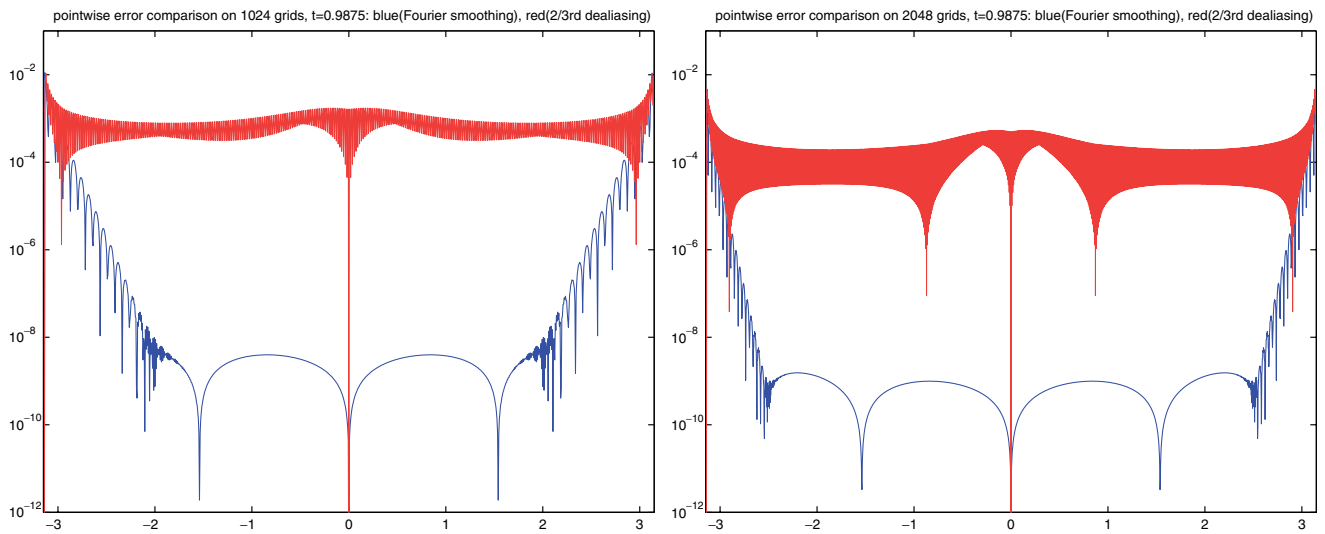


Fig. 4. The pointwise errors of the two pseudo-spectral methods as a function of time using three different resolutions. The plot is in a log scale. The initial condition is given by  $u_0(x) = \sin(x)$ . The error of the 2/3rd dealiasing method is highly oscillatory and spreads out over the entire domain, while the error of the Fourier smoothing method is highly localized near the location of the shock singularity.

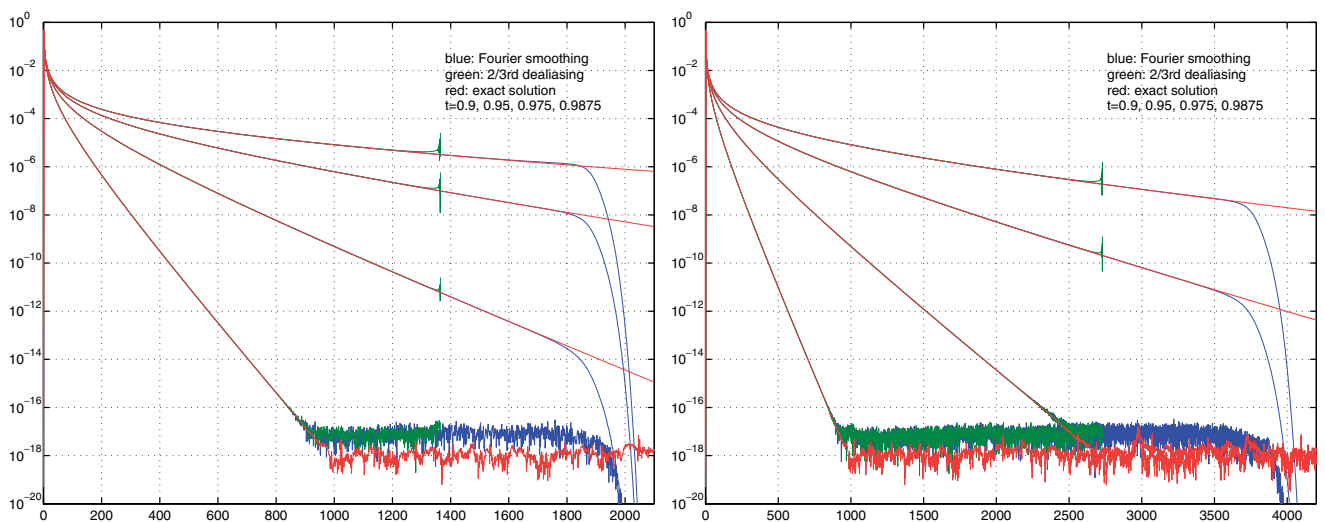


Fig. 5. Comparison of Fourier spectra of the two methods on different resolutions at a sequence of times. The initial condition is given by  $u_0(x) = \sin(x)$ . The left picture corresponds to  $N = 4096$  and the right picture corresponds to  $N = 8192$ .

with two different resolutions  $N = 4096$  and  $N = 8192$  respectively. We observe that when the solution is relatively smooth and can be resolved by the computational grid, the spectra of the two methods are almost indistinguishable. However, when the solution becomes more singular and cannot be completely resolved by the computational grid, the two methods give a very different performance. For a given resolution, the Fourier smoothing method keeps about 20% more Fourier modes than the 2/3 dealiasing method. When we compare with the “exact” spectrum obtained by using the Newton iterative method, we can see clearly that the extra Fourier modes that are kept by the Fourier smoothing method give indeed an accurate approximation to the correct Fourier modes. This explains why the Fourier smoothing method offers better accuracy than the 2/3 dealiasing method. On the other hand, we observe that the Fourier spectrum of the 2/3 dealiasing method develops noticeable oscillations near the 2/3 cut-off point of the Fourier spectrum. This abrupt cut-off in the high frequency spectrum gives rise to the well-known Gibbs phenomenon and the loss of the  $L^2$  energy, which is the main cause for the highly oscillatory and widespread pointwise error that we observe in Fig. 4.

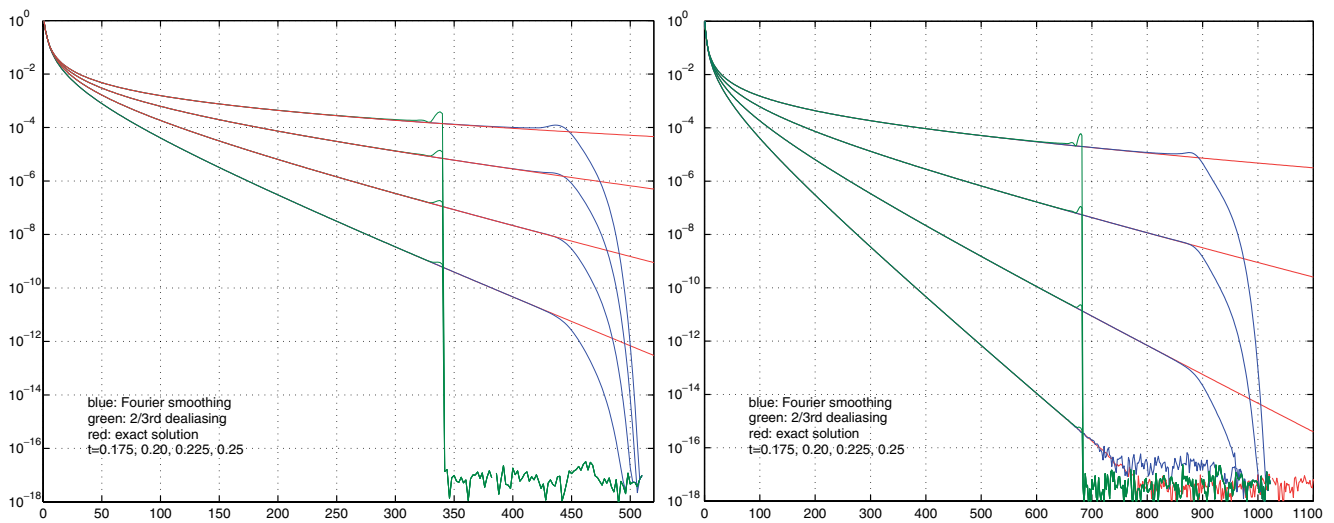


Fig. 6. Comparison of Fourier spectra of the two methods on different resolutions at a sequence of times. The initial condition is given by  $u_0(x) = (0.1 + \sin^2 x)^{-1/2}$ . The left picture corresponds to  $N = 1024$  and the right picture corresponds to  $N = 2048$ . Notice that only even modes are plotted in these figures since the odd modes are vanished in this example.

We have also performed similar numerical experiments for several other initial data. They all give the same qualitative behavior as the one we have demonstrated above. In Fig. 6, we plot the Fourier spectra of the two methods at a sequence of times using a different initial condition:  $u_0(x) = (0.1 + \sin^2 x)^{-1/2}$ . The picture on the left corresponds to resolution  $N = 1024$ , while the picture on the right corresponds to resolution  $N = 2048$ . One can see that the convergence properties of the two methods are essentially the same as those presented for the initial condition  $u_0(x) = \sin(x)$ .

Finally, we would like to point out that the numerical computations using the Fourier smoothing method have been very stable and robust. No high frequency instability has been observed throughout our computations. This indicates that the high order Fourier smoothing we use has effectively eliminated the mild numerical instability introduced by the aliasing error [13].

### 3. Computing nearly singular solutions of the 3D Euler equations using pseudo-spectral methods

In this section, we will apply the two pseudo-spectral methods to solve the nearly singular solution of the 3D incompressible Euler equations. The spectral computation of the 3D incompressible Euler equations is much more challenging due to the nonlocal and nonlinear nature of the problem and the possible formation of a finite time singularity. It would be interesting to find out if the comparison we have made regarding the convergence property of the two pseudo-spectral methods for the 1D Burgers equation is still valid for the 3D Euler equations. To make our comparison useful, we choose a smooth initial condition which could potentially develop a finite time singularity. There have been many computational efforts in searching for finite time singularities of the 3D Euler equations, see e.g. [7,27,20,16,28,18,4,2,12,26,15,19]. Of particular interest is the numerical study of the interaction of two perturbed anti-parallel vortex tubes by Kerr [18,19], in which a finite time blowup of the 3D Euler equations was reported. In this section, we will perform the comparison of the two pseudo-spectral methods using Kerr's initial condition.

The 3D incompressible Euler equations in the vorticity stream function formulation are given as follows (see e.g. [8,24]):

$$\vec{\omega}_t + (\vec{u} \cdot \nabla) \vec{\omega} = \nabla \vec{u} \cdot \vec{\omega}, \tag{6}$$

$$-\Delta \vec{\psi} = \vec{\omega}, \quad \vec{u} = \nabla \times \vec{\psi}, \tag{7}$$

with initial condition  $\vec{\omega}|_{t=0} = \vec{\omega}_0$ , where  $\vec{u}$  is velocity,  $\vec{\omega}$  is vorticity, and  $\vec{\psi}$  is stream function. Vorticity is related to velocity by  $\vec{\omega} = \nabla \times \vec{u}$ . The incompressibility implies that

$$\nabla \cdot \vec{u} = \nabla \cdot \vec{\omega} = \nabla \cdot \vec{\psi} = 0.$$

We consider periodic boundary conditions with period  $4\pi$  in all three directions. The initial condition is the same as the one used by Kerr (see Section III of [18], and also [17] for corrections of some typos in the description of the initial condition in [18]). Following [18], we call the  $x$ - $y$  plane as the “dividing plane” and the  $x$ - $z$  plane as the “symmetry plane”. There is one vortex tube above and below the dividing plane respectively. The term “anti-parallel” refers to the anti-symmetry of the vorticity with respect to the dividing plane in the following sense:  $\vec{\omega}(x, y, z) = -\vec{\omega}(x, y, -z)$ . Moreover, with respect to the symmetry plane, the vorticity is symmetric in its  $y$  component and anti-symmetric in its  $x$  and  $z$  components. Thus we have  $\omega_x(x, y, z) = -\omega_x(x, -y, z)$ ,  $\omega_y(x, y, z) = \omega_y(x, -y, z)$  and  $\omega_z(x, y, z) = -\omega_z(x, -y, z)$ . Here  $\omega_x, \omega_y, \omega_z$  are the  $x, y$ , and  $z$  components of vorticity, respectively. These symmetries allow us to compute only one quarter of the whole periodic cell.

To compare the performance of the two pseudo-spectral methods, we will perform a careful convergence study for the two methods. To get a better idea how the solution evolves dynamically, we present the 3D plot of the vortex tubes at  $t = 0$  and  $t = 6$ , respectively in Fig. 7. As we can see, the two initial vortex tubes are very smooth and essentially symmetric. Due to the mutual attraction of the two anti-parallel vortex tubes, the two vortex tubes approach to each one and experience severe deformation dynamically. By time  $t = 6$ , there is already a significant flattening near the center of the tubes. In Fig. 8, we plot the local 3D vortex structure of the upper vortex tube at  $t = 17$ . By this time, the 3D vortex tube has essentially turned into a thin vortex

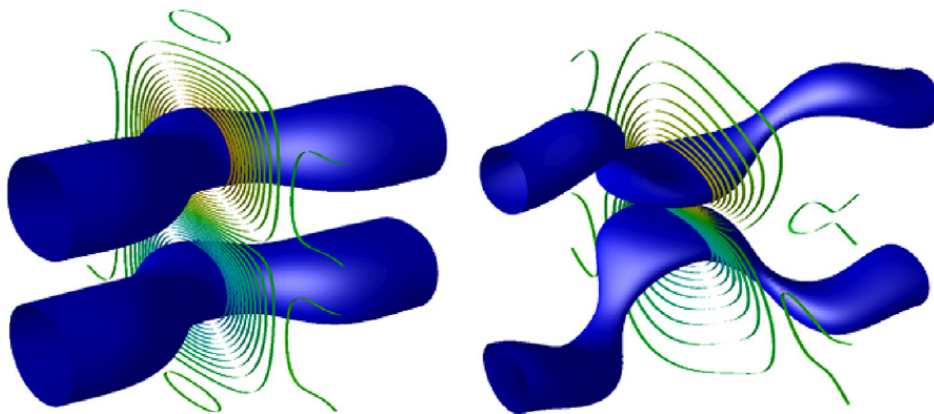


Fig. 7. The 3D view of the vortex tube for  $t = 0$  and  $t = 6$ . The tube is the isosurface at 60% of the maximum vorticity. The ribbons on the symmetry plane are the contours at other different values.

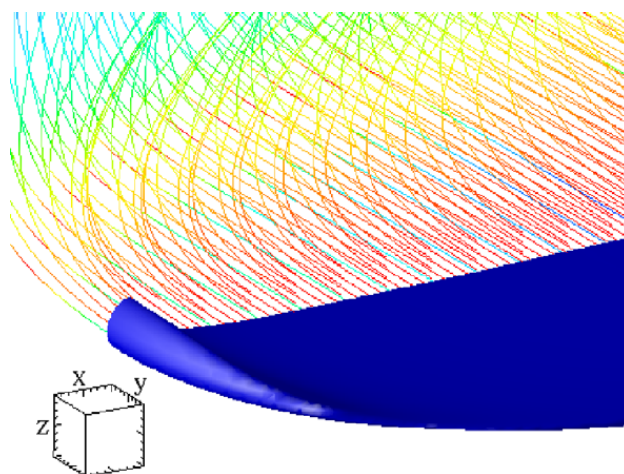


Fig. 8. The local 3D vortex structure and vortex lines around the maximum vorticity at  $t = 17$ . The size of the box on the left is  $0.075^3$  to demonstrate the scale of the picture.

sheet with rapidly decreasing thickness. The vortex sheet rolls up near the left edge of the sheet. It is interesting to note that the maximum vorticity is actually located near the rolled-up region of the vortex sheet.

### 3.1. Convergence study of the two pseudo-spectral methods in the spectral space

In this subsection, we perform a convergence study for the two numerical methods using a sequence of resolutions. For the Fourier smoothing method, we use the resolutions  $768 \times 512 \times 1536$ ,  $1024 \times 768 \times 2048$ , and  $1536 \times 1024 \times 3072$ , respectively. Except for the computation on the largest resolution  $1536 \times 1024 \times 3072$ , all computations are carried out from  $t = 0$  to  $t = 19$ . The computation on the final resolution  $1536 \times 1024 \times 3072$  is started from  $t = 10$  with the initial condition given by the computation with the resolution  $1024 \times 768 \times 2048$ . For the  $2/3$  dealiasing method, we use the resolutions  $512 \times 384 \times 1024$ ,  $768 \times 512 \times 1536$  and  $1024 \times 768 \times 2048$ , respectively. The computations using these three resolutions are all carried out from  $t = 0$  to  $t = 19$ . The time integration is performed using the classical fourth order Runge–Kutta method. Adaptive time stepping is used to satisfy the CFL stability condition with CFL number equal to  $\pi/4$ .

In Fig. 9, we compare the Fourier spectra of the energy obtained by using the  $2/3$  dealiasing method with those obtained by the Fourier smoothing method. For a fixed resolution  $1024 \times 768 \times 2048$ , we can see that the Fourier spectra obtained by the Fourier smoothing method retains more effective Fourier modes than those obtained by the  $2/3$  dealiasing method. This can be seen by comparing the results with the corresponding computations using a higher resolution  $1536 \times 1024 \times 3072$ . Moreover, the Fourier smoothing method does not give the spurious oscillations in the Fourier spectra which are present in the computations using the  $2/3$  dealiasing method near the  $2/3$  cut-off point. Similar convergence study has been made in the enstrophy spectra computed by the two methods. The results are given in Figs. 11 and 12. They give essentially the same results.

We perform further comparison of the two methods using the same resolution. In Fig. 10, we plot the energy spectra computed by the two methods using resolution  $768 \times 512 \times 1536$ . We can see that there is almost no difference in the Fourier spectra generated by the two methods in early times,  $t = 8, 10$ , when the solution is still relatively smooth. The difference begins to show near the cut-off point when the Fourier spectra rise above the round-off error level starting from  $t = 12$ . We can see that the spectra computed by the  $2/3$  dealiasing method introduces noticeable oscillations near the  $2/3$  cut-off point. The spectra computed by the Fourier smoothing method, on the other hand, extend smoothly beyond the  $2/3$  cut-off point. As we see from Figs. 10 and 9, a significant portion of those Fourier modes beyond the  $2/3$  cut-off position are still accurate. This portion of the Fourier modes that go beyond the  $2/3$  cut-off point is about 12–15% of total number

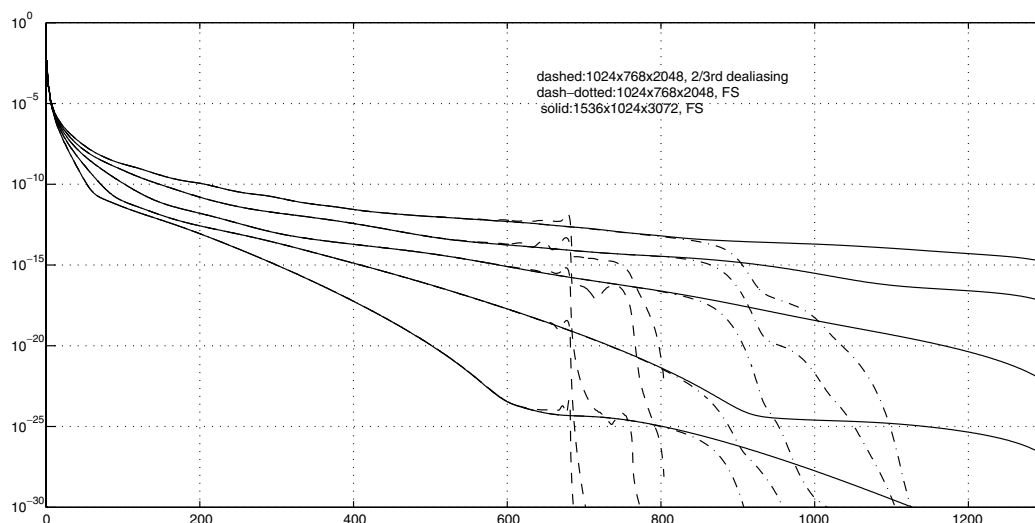


Fig. 9. The energy spectra versus wave numbers. We compare the energy spectra obtained using the Fourier smoothing method with those using the  $2/3$  dealiasing method. The dashed lines and the dashed-dotted lines are the energy spectra with the resolution  $1024 \times 768 \times 2048$  using the  $2/3$  dealiasing method and the Fourier smoothing method, respectively. The solid lines are the energy spectra obtained by the Fourier smoothing method with the highest resolution  $1536 \times 1024 \times 3072$ . The times for the spectra lines are at  $t = 15, 16, 17, 18, 19$ , respectively.

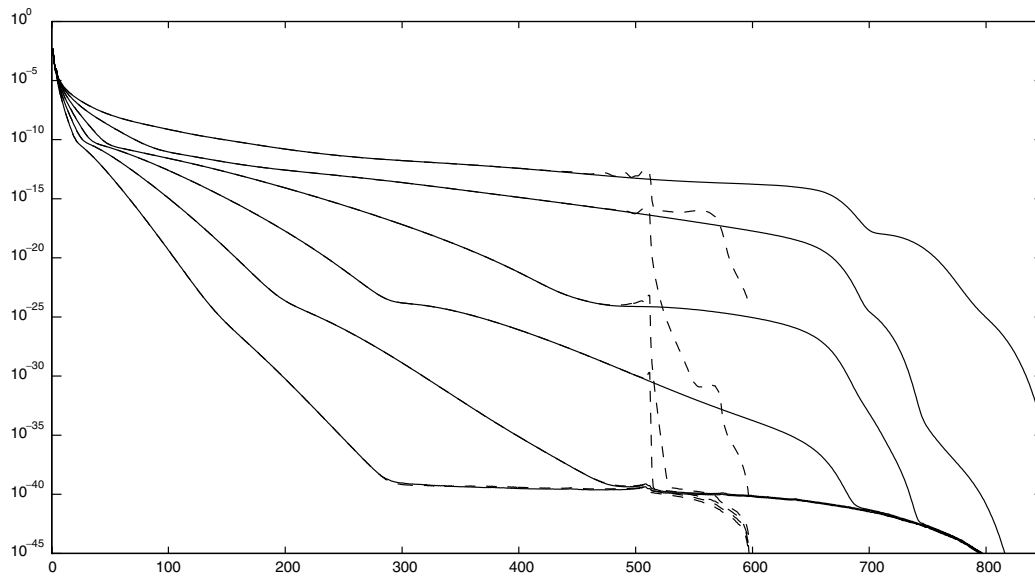


Fig. 10. The energy spectra versus wave numbers. We compare the energy spectra obtained using the Fourier smoothing method with those using the 2/3 dealiasing method. The dashed lines and solid lines are the energy spectra with the resolution  $768 \times 512 \times 1536$  using the 2/3 dealiasing method and the Fourier smoothing, respectively. The times for the spectra lines are at  $t = 8, 10, 12, 14, 16, 18$ , respectively.

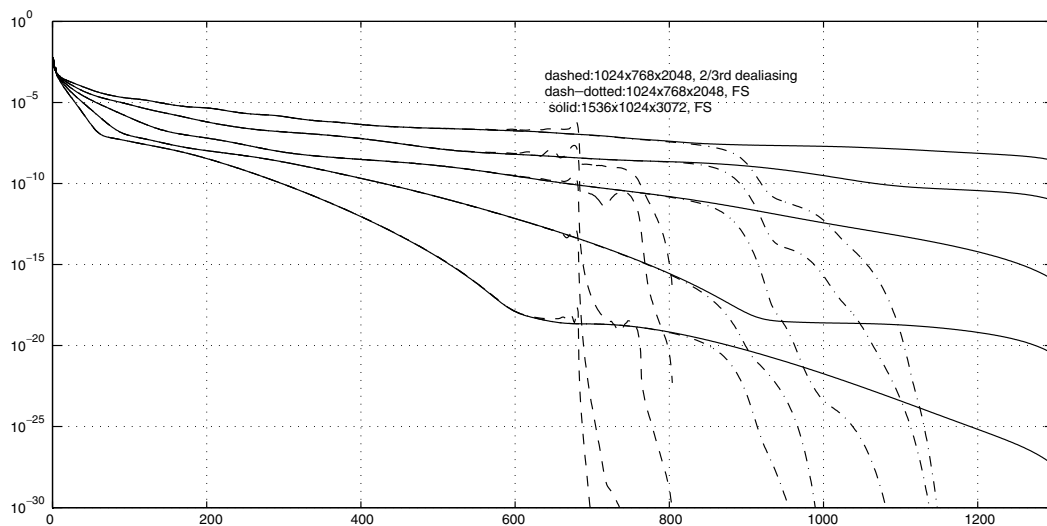


Fig. 11. The enstrophy spectra versus wave numbers. We compare the enstrophy spectra obtained using the Fourier smoothing method with those using the 2/3 dealiasing method. The dashed lines and dashed-dotted lines are the enstrophy spectra with the resolution  $1024 \times 768 \times 2048$  using the 2/3 dealiasing method and the Fourier smoothing, respectively. The solid lines are the enstrophy spectra with resolution  $1536 \times 1024 \times 3072$  obtained using the Fourier smoothing. The times for the spectra lines are at  $t = 15, 16, 17, 18, 19$ , respectively.

of modes in each dimension. For 3D problems, the total number of effective modes in the Fourier smoothing method is about 20% more than that in the 2/3 dealiasing method. This is a very significant increase in the resolution for a large scale computation. In our largest resolution, the effective Fourier modes in our Fourier smoothing method are more than 320 millions, which has 140 millions more effective modes than the corresponding 2/3 dealiasing method.

### 3.2. Comparison of the two methods in the physical space

Next, we compare the solutions obtained by the two methods in the physical space for the velocity field and the vorticity. In Fig. 13, we compare the maximum velocity as a function of time computed by the two

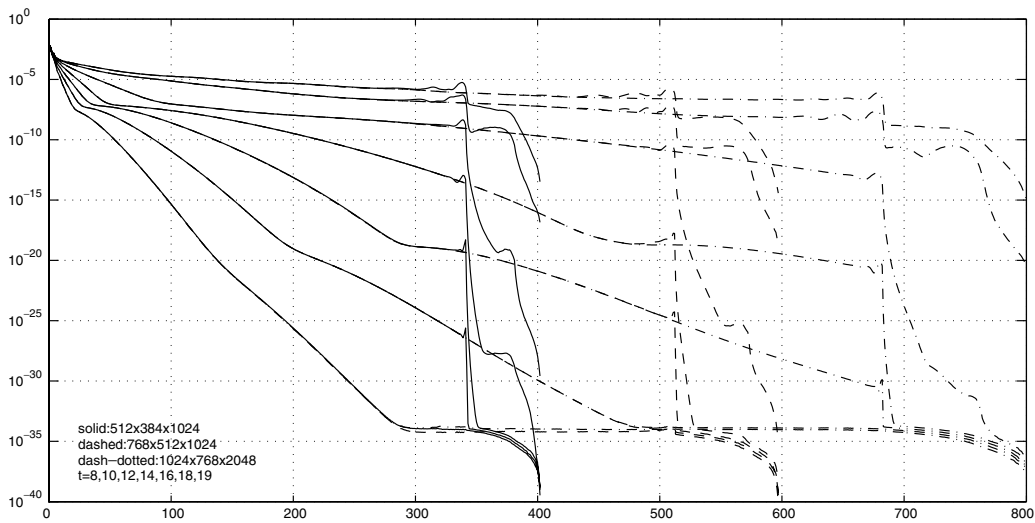


Fig. 12. Convergence study for enstrophy spectra obtained by the 2/3 dealiasing method using different resolutions. The solid line is computed with resolution  $512 \times 384 \times 1024$ , the dashed line is computed with resolution  $768 \times 512 \times 1536$ , and the dashed-dotted line is computed with resolution  $1024 \times 768 \times 2048$ . The times for the lines from bottom to top are  $t = 8, 10, 12, 14, 16, 18, 19$ .

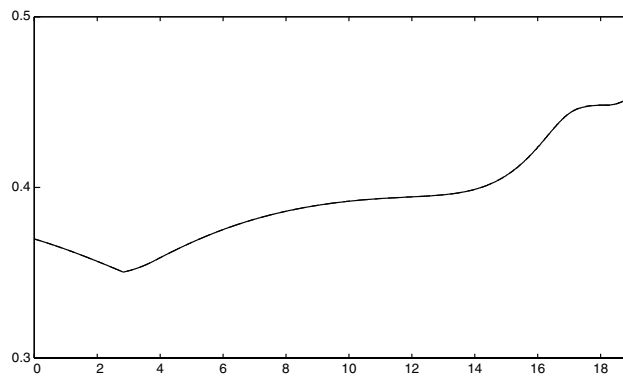


Fig. 13. Comparison of maximum velocity as a function of time computed by two methods. The solid line represents the solution obtained by the Fourier smoothing method, and the dashed line represents the solution obtained by the 2/3 dealiasing method. The resolution is  $1024 \times 768 \times 2048$  for both methods.

methods using resolution  $1024 \times 768 \times 2048$ . The two solutions are almost indistinguishable. In Fig. 14, we plot the maximum vorticity as a function of time. The two solutions also agree reasonably well. However, the comparison of the solutions obtained by the two methods at resolutions lower than  $1024 \times 768 \times 2048$  shows more significant differences of the two methods, see Figs. 15, 19 and 20.

To understand better how the two methods differ in their performance, we examine the contour plots of the axial vorticity in Figs. 16–18. As we can see, the vorticity computed by the 2/3 dealiasing method already develops small oscillations at  $t = 17$ . The oscillations grow bigger by  $t = 18$  (see Fig. 17), and bigger still at  $t = 19$  (see Fig. 18). We note that the oscillations in the axial vorticity contours concentrate near the region where the magnitude of vorticity is close to zero. Thus they have less an effect on the maximum vorticity. On the other hand, the solution computed by the Fourier smoothing method is still relatively smooth.

To further demonstrate the accuracy of our computations we compare the maximum vorticity obtained by the Fourier smoothing method for three different resolutions:  $768 \times 512 \times 1536$ ,  $1024 \times 768 \times 2048$ , and  $1536 \times 1024 \times 3072$ , respectively. The result is plotted in Fig. 19. We have performed a similar convergence study for the 2/3 dealiasing method for the maximum vorticity. The result is given in Fig. 20. Two conclusions can be made from this resolution study. First, by comparing Fig. 19 with Fig. 20, we can see that the Fourier

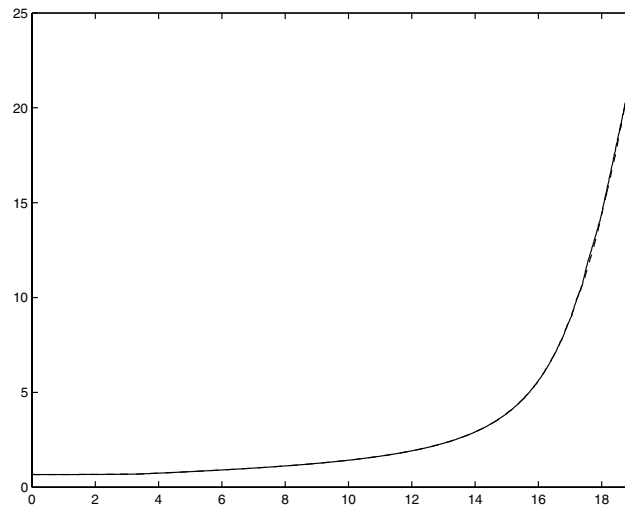


Fig. 14. Comparison of maximum vorticity as a function of time computed by two methods. The solid line represents the solution obtained by the Fourier smoothing method, and the dashed line represents the solution obtained by the  $2/3$  dealiasing method. The resolution is  $1024 \times 768 \times 2048$  for both methods.

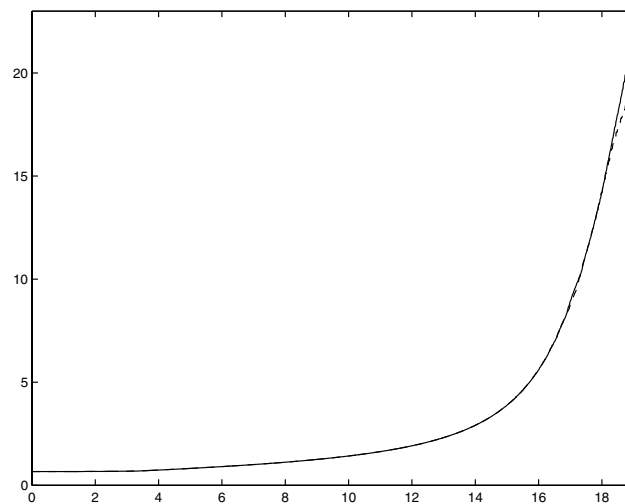


Fig. 15. Comparison of maximum vorticity as a function of time computed by two methods. The solid line represents the solution obtained by the Fourier smoothing method, and the dashed line represents the solution obtained by the  $2/3$  dealiasing method. The resolution is  $768 \times 512 \times 1024$  for both methods.

smoothing method is indeed more accurate than the  $2/3$  dealiasing method for a given resolution. The  $2/3$  dealiasing method gives a slower growth rate in the maximum vorticity with resolution  $768 \times 512 \times 1536$ . Secondly, the resolution  $768 \times 512 \times 1536$  is not good enough to resolve the nearly singular solution at later times. On the other hand, we observe that the difference between the numerical solution obtained by the resolution  $1024 \times 768 \times 2048$  and that obtained by the resolution  $1536 \times 1024 \times 3072$  is relatively small. This indicates that the vorticity is reasonably well-resolved by our largest resolution  $1536 \times 1024 \times 3072$ .

We have also performed a similar resolution study for the maximum velocity in Fig. 23. The solutions obtained by the two largest resolutions are almost indistinguishable, which suggests that the velocity is well-resolved by our largest resolution  $1536 \times 1024 \times 3072$ .

The resolution study given by Figs. 15 and 20 also suggests that the computation obtained by the pseudo-spectral method with the  $2/3$  dealiasing rule using resolution  $768 \times 512 \times 1536$  is significantly under-resolved after  $t = 18$ . It is interesting to note from Fig. 15 that the computational results obtained by the two methods

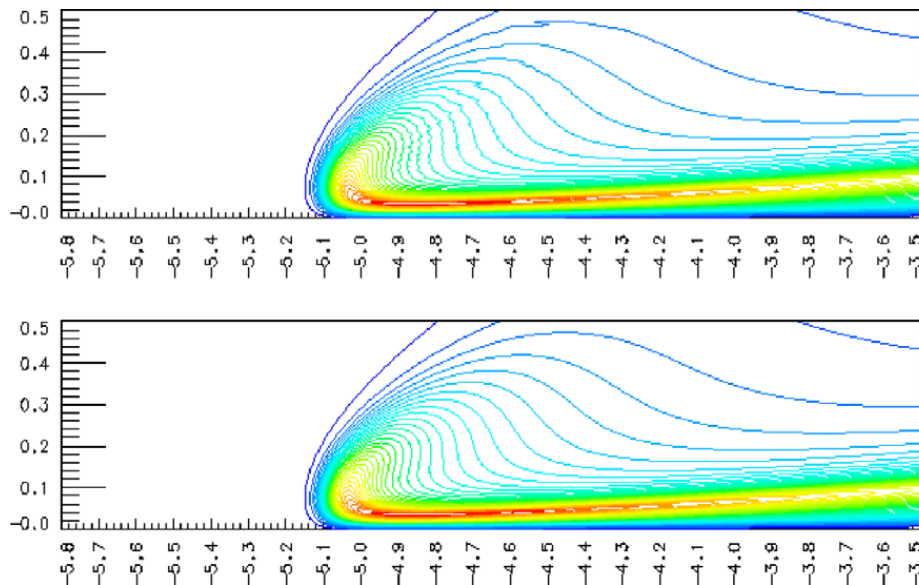


Fig. 16. Comparison of axial vorticity contours at  $t = 17$  computed by two methods. The upper picture is the solution obtained by the 2/3 dealiasing method, and the picture on the bottom is the solution obtained by the Fourier smoothing method. The resolution is  $1024 \times 768 \times 2048$  for both methods.

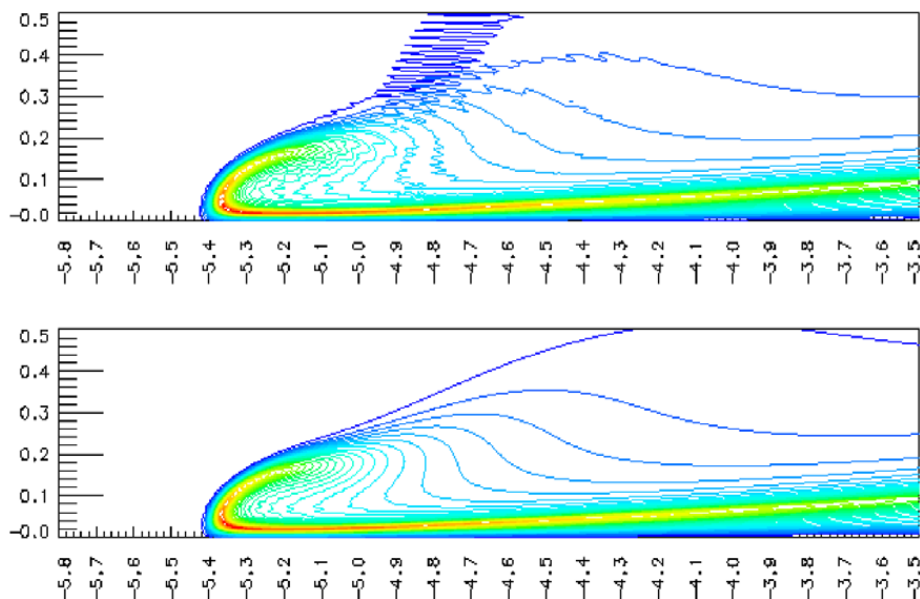


Fig. 17. Comparison of axial vorticity contours at  $t = 18$  computed by two methods. The upper picture is the solution obtained by the 2/3 dealiasing method, and the picture on the bottom is the solution obtained by the Fourier smoothing method. The resolution is  $1024 \times 768 \times 2048$  for both methods.

with resolution  $768 \times 512 \times 1536$  begin to deviate from each other precisely around  $t = 18$ . By comparing the result from Fig. 15 with that from Fig. 19, we confirm again that for a given resolution, the Fourier smoothing method gives a more accurate approximation than the 2/3 dealiasing method.

We remark that our numerical computations for the 3D incompressible Euler equations using the Fourier smoothing method are very stable and robust. No high frequency instability has been observed. In the case of the 3D Euler equations, the energy is conserved up to at least six digits of accuracy throughout the computations. The resolution study we perform here is completely based on the consideration of accuracy, not on stability. This again confirms that the Fourier smoothing method offers a very stable and accurate computational method for the 3D incompressible flow.

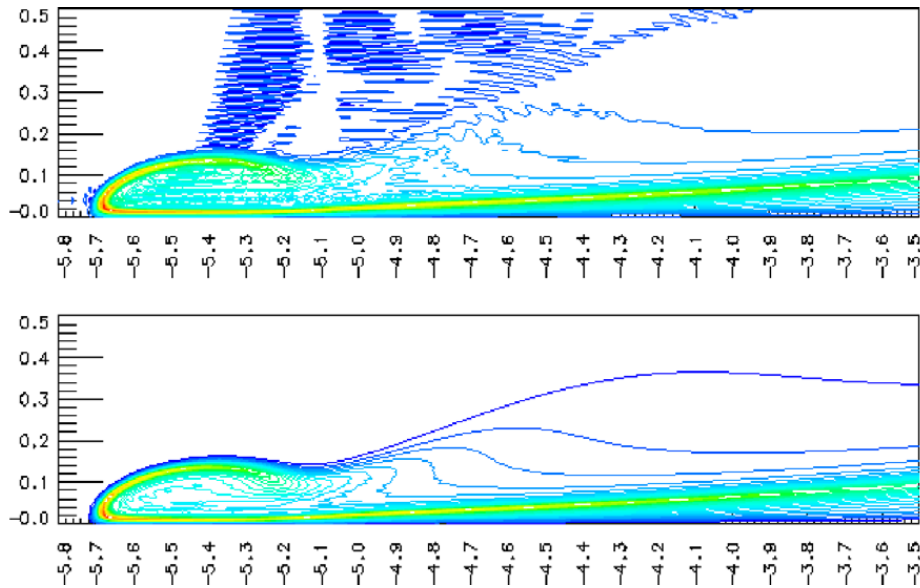


Fig. 18. Comparison of axial vorticity contours at  $t = 19$  computed by two methods. The upper picture is the solution obtained by the 2/3 dealiasing method, and the picture on the bottom is the solution obtained by the Fourier smoothing method. The resolution is  $1024 \times 768 \times 2048$  for both methods.

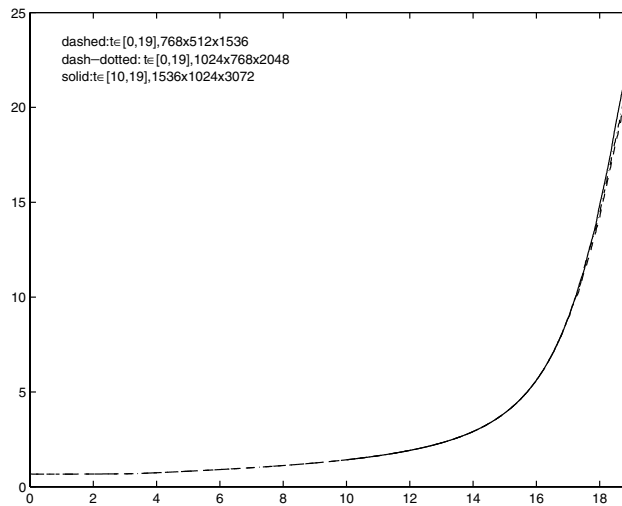


Fig. 19. The maximum vorticity  $\|\vec{\omega}\|_\infty$  in time computed by the Fourier smoothing method using different resolutions.

### 3.3. Does a finite time singularity develop?

Before we conclude this section, we would like to have further discussions how to interpret the numerical results we have obtained. Specifically, given the fast growth of maximum vorticity, does a finite time singularity develop for this initial condition?

In [18], Kerr presented numerical evidence which suggested a finite time singularity of the 3D Euler equations for the same initial condition that we use in this paper. Kerr used a pseudo-spectral discretization with the 2/3 dealiasing rule in the  $x$  and  $y$  directions, and a Chebyshev method in the  $z$  direction with resolution of order  $512 \times 256 \times 192$ . His computations showed that the growth of the peak vorticity, the peak axial strain, and the enstrophy production obey  $(T - t)^{-1}$  with  $T = 18.9$ . In his recent paper [19], Kerr applied a high wave number filter to the data obtained in his original computations to “remove the noise that masked the structures in earlier graphics” presented in [18]. With this filtered solution, he presented some scaling analysis of the numerical solutions up to  $t = 17.5$ . Two new properties were presented in this recent paper [19]. First, the

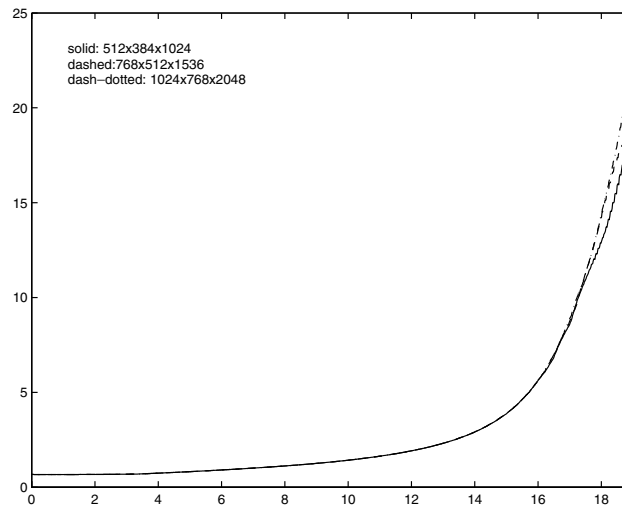


Fig. 20. The maximum vorticity  $\|\vec{\omega}\|_\infty$  in time computed by the 2/3 dealiasing method using different resolutions.

velocity field was shown to blow up like  $O(T - t)^{-1/2}$  with  $T$  being revised to  $T = 18.7$ . Secondly, he showed that the blowup is characterized by two anisotropic length scales,  $\rho \approx (T - t)$  and  $R \approx (T - t)^{1/2}$ .

From the resolution study we present in Fig. 19, we find that the maximum vorticity increases rapidly from the initial value of 0.669 to 23.46 at the final time  $t = 19$ , a factor of 35 increase from its initial value. Kerr's computations predicted a finite time singularity at  $T = 18.7$ . Our computations show no sign of finite time blowup of the 3D Euler equations up to  $T = 19$ , beyond the singularity time predicted by Kerr. From Figs. 16–18, we can see that a thin layer (or a vortex sheet) is formed dynamically. Beyond  $t = 17$ , the vortex sheet has rolled up and traveled backward for some distance. With only 192 grid points along the  $z$ -direction, Kerr's computations did not have enough grid points to resolve the nearly singular vortex sheet that travels backward and away from the  $z$ -axis. In comparison, we have 3072 grid points along the  $z$ -direction. This gives about 16 grid points across the nearly singular layered structure at  $t = 18$  and about +8 grid points at  $t = 19$ .

In order to understand the nature of the dynamic growth in vorticity, we examine the degree of nonlinearity in the vortex stretching term. In Fig. 21, we plot the quantity,  $\|\xi \cdot \nabla \vec{u} \cdot \vec{\omega}\|_\infty$ , as a function of time, where  $\xi$  is the unit vorticity vector. If the maximum vorticity indeed blew up like  $O((T - t)^{-1})$ , as alleged in [18], this quantity should have been quadratic as a function of maximum vorticity. We find that there is tremendous cancellation in this vortex stretching term. It actually grows slower than  $C\|\vec{\omega}\|_\infty \log(\|\vec{\omega}\|_\infty)$ , see Fig. 21. It

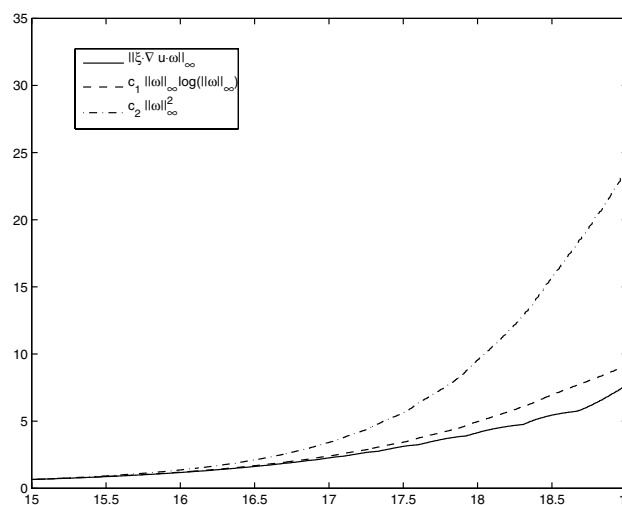


Fig. 21. Study of the vortex stretching term in time. This computation is performed by the Fourier smoothing method with resolution  $1536 \times 1024 \times 3072$ . We take  $c_1 = 1/8.128$ ,  $c_2 = 1/23.24$  to match the same starting value for all three plots.

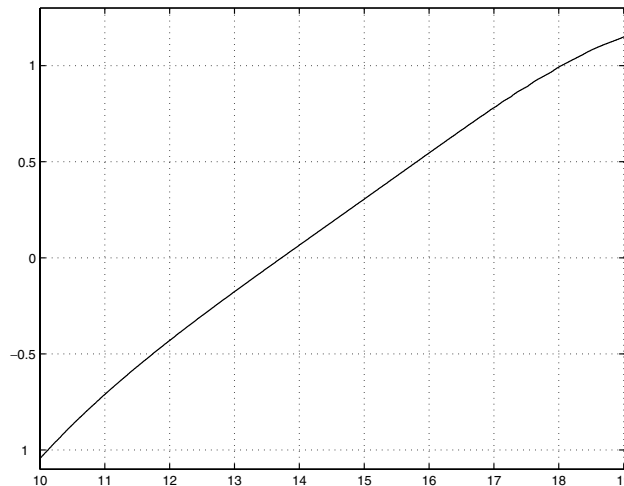


Fig. 22. The plot of  $\log\text{-}\log \|\omega\|_\infty$  vs time. This computation is performed by the Fourier smoothing method with resolution  $1536 \times 1024 \times 3072$ .

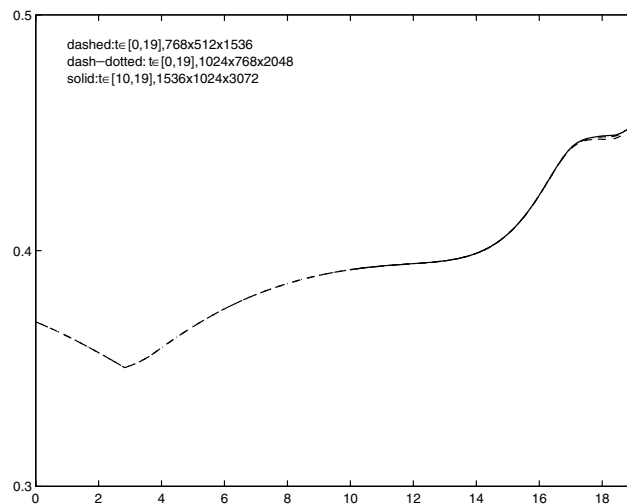


Fig. 23. Maximum velocity  $\|\vec{u}\|_\infty$  in time computed by the Fourier smoothing method using different resolutions.

is easy to show that such weak nonlinearity in vortex stretching would imply only doubly exponential growth in the maximum vorticity. Indeed, as demonstrated by Fig. 22, the maximum vorticity does not grow faster than doubly exponential in time. In fact, a closer inspection reveals that the location of the maximum vorticity has moved away from the dividing plane for  $t \geq 17.5$ . This implies that the compression mechanism between the two vortex tubes becomes weaker toward the end of the computation, leading to a slower growth rate in maximum vorticity [17].

Another important evidence which supports the non-blowup of the solution up to  $t = 19$  is that the maximum velocity remains bounded, see Fig. 23. This is in contrast with the claim in [19] that the maximum velocity blows up like  $O(T - t)^{-1/2}$  with  $T = 18.7$ . With the velocity field being bounded, the local non-blowup criteria of Deng–Hou–Yu [10,11] can be applied, which implies that the solution of the 3D Euler equations remains smooth at least up to  $T = 19$ , see also [17].

#### 4. Conclusion remarks

In this paper, we have performed a systematic convergence study of the two pseudo-spectral methods. The first pseudo-spectral method uses the traditional 2/3 dealiasing rule, while the second pseudo-spectral method

uses a high order Fourier smoothing. The Fourier smoothing method is designed to cut off the high frequency modes smoothly while retaining a significant portion of the Fourier modes beyond the  $2/3$  cut-off point in the spectral space. We apply both methods to compute nearly singular solutions of the 1D Burgers equation and the 3D incompressible Euler equations. In the case of the 1D Burgers equation, we can obtain a very accurate approximation of the exact solution sufficiently close to the singularity time with 13 digits of accuracy. This allows us to estimate the numerical errors of the two methods accurately and provides a solid ground in our convergence study. In our study of the 3D incompressible Euler equations, we use the highest resolution that we can afford to perform our convergence study. In both cases, we demonstrate convincingly that the Fourier smoothing method gives a more accurate approximation than the  $2/3$  dealiasing method.

Our extensive convergence studies in both physical and spectral spaces show that the Fourier smoothing method offers several advantages over the  $2/3$  dealiasing method when computing a nearly singular solution. First of all, the error in the Fourier smoothing method is highly localized near the region where the solution is most singular. The error in the smooth region is several orders of magnitude smaller than that near the “singular” region. The  $2/3$  dealiasing method, on the other hand, has a wide spread pointwise error distribution, and produces relatively large oscillations even in the smooth region. Secondly, for the same resolution, the Fourier smoothing method offers a more accurate approximation to the physical solution than the  $2/3$  dealiasing method. Our numerical study shows that for a given resolution, the Fourier smoothing method retains about 12–15% more effective Fourier modes than the  $2/3$  dealiasing method in each dimension. For a 3D problem, the gain is as large as 20%. This gain is quite significant in a large scale computation. Thirdly, the Fourier smoothing method is very stable and robust when computing nearly singular solutions of fluid dynamics equations. Spectral convergence is clearly observed in all our computational experiments without suffering from the Gibbs phenomenon. Moreover, there is no additional computational cost in implementing the Fourier smoothing method. We have also implemented the Fourier smoothing method for the incompressible 3D Navier–Stokes equations and observed a similar performance.

We have applied both spectral methods to study the potentially singular solution of the 3D Euler equation using the same initial condition as Kerr [18]. Both the Fourier smoothing method and the  $2/3$  dealiasing method give qualitatively the same result except that the  $2/3$  dealiasing method suffers from the Gibbs phenomenon and produces relative large oscillations at late times. Our convergence study in both the physical and spectral spaces shows that the maximum vorticity does not grow faster than double exponential in time and the maximum velocity field remains bounded up to  $T = 19$ , beyond the singularity time  $T = 18.7$  alleged in [18,19]. Tremendous cancellation seems to take place in the vortex stretching term. The local geometric regularity of the vortex lines near the region of the maximum vorticity seems to be responsible for this dynamic depletion of vortex stretching [9–11,17].

## Acknowledgments

We thank Prof. Lin-Bo Zhang from the Institute of Computational Mathematics in Chinese Academy of Sciences (CAS) for providing us with the computing resource to perform this large scale computational project. Additional computing resource was provided by the Center of High Performance Computing in CAS. We also thank Prof. Robert Kerr for providing us with his Fortran subroutine that generates his initial data. This work was in part supported by NSF under the NSF FRG Grant DMS-0353838 and ITR Grant ACI-0204932. Part of this work was done while Hou visited the Academy of Systems and Mathematical Sciences of CAS in the summer of 2005 as a member of the Oversea Outstanding Research Team for Complex Systems. Li was supported by the National Basic Research Program of China under the Grant 2005CB321701. Finally, we thank Professors Alfio Quarteroni, Jie Shen, and Eitan Tadmor for their valuable comments on our draft manuscript.

## References

- [1] S. Abarbanel, D. Gottlieb, E. Tadmor, Spectral methods for discontinuous problems, in: K.W. Morton, M.J. Baines (Eds.), *Numerical Methods for Fluid Dynamics II*, Clarendon Press, 1986, pp. 129–153.
- [2] O.N. Boratav, R.B. Pelz, Direct numerical simulation of transition to turbulence from a high-symmetry initial condition, *Phys. Fluids* 6 (8) (1994) 2757–2784.

- [3] J.P. Boyd, *Chebyshev and Fourier Spectral Methods*, second ed., Dover Publications, Inc, New York, 2000.
- [4] R. Caflisch, Singularity formation for complex solutions of the 3D incompressible Euler equations, *Physica D* 67 (1993) 1–18.
- [5] C. Canuto, M.Y. Hussaini, A. Quarteroni, T.A. Zang, *Spectral Methods in Fluid Dynamics*, Springer, Berlin, 1988.
- [6] C. Canuto, M.Y. Hussaini, A. Quarteroni, T.A. Zang, *Spectral Methods: Fundamentals in Single Domains*, Springer, Berlin, 2006.
- [7] A. Chorin, The evolution of a turbulent vortex, *Commun. Math. Phys.* 83 (1982) 517.
- [8] A.J. Chorin, J.E. Marsden, *A Mathematical Introduction to Fluid Mechanics*, third ed., Springer, New York, 1993.
- [9] P. Constantin, C. Fefferman, A. Majda, Geometric constraints on potentially singular solutions for the 3-D Euler equation, *Comm. PDEs* 21 (1996) 559–571.
- [10] J. Deng, T.Y. Hou, X. Yu, Geometric properties and non-blowup of 3-D incompressible Euler flow, *Comm. PDEs* 30 (1) (2005) 225–243.
- [11] J. Deng, T.Y. Hou, X. Yu, Improved geometric conditions for non-blowup of 3D incompressible Euler equation, *Comm. PDEs* 31 (2) (2006) 293–306.
- [12] V.M. Fernandez, N.J. Zabusky, V.M. Gryanik, Vortex intensification and collapse of the Lissajous-elliptic ring: single and multi-filament Biot–Savart simulations and visimetrics, *J. Fluid Mech.* 299 (1995) 289–331.
- [13] J. Goodman, T.Y. Hou, E. Tadmor, On the stability of the unsmoothed Fourier method for hyperbolic equations, *Numer. Math.* 67 (1994) 93–129.
- [14] D. Gottlieb, S.A. Orszag, *Numerical Analysis of Spectral Methods: Theory and Applications*, SIAM, Philadelphia, 1989.
- [15] R. Grauer, C. Marliani, K. Germaschewski, Adaptive mesh refinement for singular solutions of the incompressible Euler equations, *Phys. Rev. Lett.* 80 (1998) 19.
- [16] R. Grauer, T. Sideris, Numerical computation of three dimensional incompressible ideal fluids with swirl, *Phys. Rev. Lett.* 67 (1991) 3511.
- [17] T.Y. Hou, R. Li, Dynamic depletion of vortex stretching and non-blowup of the 3-D incompressible Euler equations, *J. Nonlinear Sci.* 16 (6) (2006) 639–664.
- [18] R.M. Kerr, Evidence for a singularity of the three dimensional, incompressible Euler equations, *Phys. Fluids* 5 (7) (1993) 1725–1746.
- [19] R.M. Kerr, Velocity and scaling of collapsing Euler vortices, *Phys. Fluids* 17 (2005), 075103-114.
- [20] R.M. Kerr, F. Hussain, Simulation of vortex reconnection, *Physica D* 37 (1989) 474.
- [21] R.J. LeVeque, *Numerical Method for Conservation Laws*, Birkhäuser, 1992.
- [22] Y. Maday, E. Tadmor, Analysis of the spectral vanishing viscosity method for periodic conservation laws, *SINUM* 26 (1989) 854–870.
- [23] A. Majda, J. McDonough, S. Osher, The Fourier method for nonsmooth initial data, *Math. Comput.* 32 (1978) 1041–1081.
- [24] A.J. Majda, A.L. Bertozzi, *Vorticity and Incompressible Flow*, Cambridge University Press, Cambridge, 2002.
- [25] M.S. Mock, P.D. Lax, The computation of discontinuous solutions of linear hyperbolic equations, *CPAM* 31 (1978) 423–430.
- [26] R.B. Pelz, Locally, self-similar finite-time collapse in a high-symmetry vortex filament model, *Phys. Rev. E* 55 (2) (1997) 1617–1626.
- [27] A. Pumir, E.E. Siggia, Collapsing solutions to the 3-D Euler equations, *Phys. Fluids A* 2 (1990) 220–241.
- [28] M.J. Shelley, D.I. Meiron, S.A. Orszag, Dynamical aspects of vortex reconnection of perturbed anti-parallel vortex tubes, *J. Fluid Mech.* 246 (1993) 613–652.
- [29] E. Tadmor, Convergence of spectral methods for nonlinear conservation laws, *SINUM* 26 (1989) 30–44.
- [30] E. Tadmor, Super viscosity and spectral approximations of nonlinear conservation laws, in: M.J. Baines, K.W. Morton (Eds.), *Numerical Methods for Fluid Dynamics IV*, Clarendon Press, 1993, pp. 69–82.